

Triggered Star Formation in Galaxy Pairs at $z = 0.08 - 0.38$ (Short title: “Triggered Star Formation”)

Deborah Freedman Woods

Department of Astronomy, Harvard University, Cambridge, MA 02138

dwoods@cfa.harvard.edu

Margaret J. Geller, Michael J. Kurtz,

Eduard Westra, Daniel G. Fabricant

Smithsonian Astrophysical Observatory, Cambridge, MA 02138

Ian Dell’Antonio

Department of Physics, Brown University, Providence, RI 02912

ABSTRACT

We measure the strength, frequency, and timescale of tidally triggered star formation at redshift $z = 0.08 - 0.38$ in a spectroscopically complete sample of galaxy pairs drawn from the magnitude-limited redshift survey of 9,825 Smithsonian Hectospec Lensing Survey (SHELS) galaxies with $R < 20.3$. To examine the evidence for tidal triggering, we identify a volume-limited sample of major ($|\Delta M_R| < 1.75$, corresponding to mass ratio $> 1/5$) pair galaxies with $M_R < -20.8$ in the redshift range $z = 0.08 - 0.31$. The size and completeness of the spectroscopic survey allows us to focus on regions of low local density. The spectrophotometric calibration enables the use of the the 4000 Å break (D_n4000), the $H\alpha$ specific star formation rate ($SSFR_{H\alpha}$), and population models to characterize the galaxies. We show that D_n4000 is a useful population classification tool; it closely tracks the identification of emission line galaxies. The sample of major pair galaxies in regions of low local density with low D_n4000 demonstrates the expected anti-correlation between pair-wise projected separation and a set of star formation indicators explored in previous studies. We measure the frequency of triggered star formation by comparing the $SSFR_{H\alpha}$ in the volume-limited sample in regions of low local density: $32 \pm 7\%$ of the major pair galaxies have $SSFR_{H\alpha}$ at least double the median rate of the unpaired field galaxies. Comparison of stellar population models for pair and for unpaired field galaxies implies a timescale for triggered star formation of $\sim 300 - 400$ Myr.

Subject headings: galaxies: interactions – galaxies: stellar content – galaxies: active

1. Introduction

Hierarchical galaxy formation models predict frequent interactions in a galaxy’s history (e.g. Cole et al. 2000; Wechsler et al. 2002). Some of these interactions may trigger star formation. Observational limits on the frequency and duration

of triggered star formation are an important constraint on the role of these interactions in the evolution of stellar populations.

Evidence that galaxy interactions at low redshift trigger star formation was first detected in photometric observations by Larson & Tinsley

(1978), who demonstrated that apparently interacting galaxies in the Atlas of Peculiar Galaxies (Arp 1966) have a broader range of colors and tidal features than typical galaxies. Spectroscopic indicators confirm that interacting galaxies tend to have enhanced star formation rates (Kennicutt & Keel 1984; Kennicutt et al. 1987; Keel 1993; Liu & Kennicutt 1995a; Donzelli & Pastoriza 1997; Barton et al. 2000, 2003; Lambas et al. 2003; Nikolic et al. 2004; Kauffmann et al. 2004; Woods et al. 2006; Woods & Geller 2007; Ellison et al. 2008). Infrared observations (Kennicutt et al. 1987; Jones & Stein 1989; Sekiguchi & Wolstencroft 1992; Keel 1993; Nikolic et al. 2004; Geller et al. 2006; Smith et al. 2007) and radio observations (Hummel 1981) yield similar results. Observations that galaxy pairs with the smallest project separation have the highest star formation rates provide direct evidence for triggered star formation (e.g Barton et al. 2000).

Recent studies show that galaxy interactions at intermediate redshift trigger star formation. Measurements of infrared luminosity (Lin et al. 2007) and $\text{EW}([\text{O II}])$ (de Ravel et al. 2009) indicate an anti-correlation between projected separation and star formation activity for pair galaxies at intermediate redshift ($z < 1$), similar to the trend observed at low redshift. Analysis of the morphology of intermediate redshift ($z = 0.1 - 0.6$) pair galaxies likewise shows an increase in the fraction of asymmetric galaxies in pairs, an indication of tidal interaction (Patton et al. 2005).

Although observations demonstrate that galaxy interactions *can* lead to enhanced star formation activity, the results of studies of the frequency and intensity of star formation activity appear to vary with the sample selection. Li et al. (2008a) find that 30% of the SDSS pair galaxies with high specific star formation rates have a companion within 100 kpc, and that low to average specific star formation rate galaxies rarely have a companion. In a separate study of SDSS pair galaxies at $z < 0.16$, Ellison et al. (2008) measure up to 40% enhancement in the median star formation rate of close pair galaxies with stellar mass ratios $< 1/10$ relative to their comparison sample of non-pair systems. Bergvall et al. (2003) find that global UBV colors do not show significant enhancement in star formation in their small sample of interacting galaxies compared to isolated sys-

tems. However, they do find that star formation rates at the very centers of the interacting systems are increased by a factor of $\sim 2 - 3$ over the non-interacting systems. Spitzer infrared observations of 35 tidally disturbed Arp galaxies show that their $24 \mu\text{m}$ emission is more centrally concentrated than in normal spiral galaxies, suggesting a build up of central gas which could fuel central star formation; their infrared colors suggest an increase in the mass normalized SFR by a factor of two over the normal spirals (Smith et al. 2007).

Numerical simulations account for the observed range of strength, frequency, and duration of triggered star formation. In the large suite of simulations by Di Matteo et al. (2008), galaxy interactions and mergers produce only moderate star formation enhancement relative to non-interacting galaxies at low redshift. Strong starbursts are rare and short lived, typically lasting a few hundred Myr. The duration of the starburst declines as the enhancement in star formation rate increases.

Global galaxy properties affect their susceptibility to tidally triggered star formation. Systems with sufficient gas can exhibit triggered star formation in major interactions (e.g. Mihos & Hernquist 1996; Tissera et al. 2002; Cox et al. 2006; Di Matteo et al. 2007). Interactions between gas-poor galaxies (“dry mergers”) produce little or no star formation, although they contribute substantially to the build-up of massive galaxies (e.g. Tran et al. 2005; Van Dokkum 2005; Cattaneo et al. 2008). Internal structure strongly affects the susceptibility to gaseous inflows; late-type galaxies without strong bulge components are more likely to have bar instabilities that drive the gaseous inflows powering the central star formation (Mihos & Hernquist 1996; Di Matteo et al. 2007).

The relative mass of the galaxy compared to its neighbor and the intrinsic mass also influence the degree of triggered star formation. Galaxy pairs of similar mass (luminosity) show strong enhancement to their star formation rates in both members of the pair in both observational (Woods & Geller 2007; Ellison et al. 2008) and theoretical (Cox et al. 2008) studies. Observations show that although satellite galaxies occasionally experience triggered star formation, the brighter of a high mass (luminosity) ratio pair does not undergo significant tidal triggering (Woods & Geller 2007); numerical simulations suggest a similar pic-

ture (Cox et al. 2008). The intrinsic mass of the galaxy also plays a role: low mass (luminosity) galaxies in major mergers are more strongly affected by the interaction than are high mass galaxies in major mergers in observations of pair galaxies (Woods & Geller 2007; Ellison et al. 2008).

Local environment can affect star formation activity in a galaxy apparently independent of an interaction. Galaxies in clusters and large groups tend to have redder color and less current star formation than isolated systems (e.g. Hubble & Humason 1931; Cooper et al. 2007; Gerke et al. 2007). Barton et al. (2007) show that pair galaxies are more common in regions with greater local density than are unpaired galaxies. Including pair galaxies from high density regions suppresses the signal of triggered star formation measured in comparison to unpaired galaxies.

We take advantage of the size and completeness of the Smithsonian Hectospec Lensing Survey (SHELS, Geller et al. 2005, 2010) galaxy sample to identify a set of major interactions at $z = 0.08 - 0.38$ for galaxies with young stellar populations in regions of low local density, where we can measure the cleanest signal of triggered star formation. Local density selection at intermediate redshift has not been possible before this sample.

The stability of the Hectospec instrument enable accurate spectrophotometric calibration of the spectra. The calibrated spectra provide the 4000 Å break (D_n4000) and the $H\alpha$ specific star formation rate ($SSFR_{H\alpha}$), which we use to characterize the star formation. We quantify the frequency, strength, and timescale of triggered star formation in major galaxy interactions using measurement of specific star formation rates and stellar population models fitted to the individual spectra.

We describe the SHELS data in §2 and the sample selection in §3. Section 4 describes the classification of galaxies as starforming or AGN and the use of the spectroscopic indicator D_n4000 to identify galaxy types. We consider local density effects in §5. Section 6 describes various measurements of tidally triggered star formation, including the frequency, strength, and timescale of enhanced star formation activity. Throughout this study we assume standard Λ CDM cosmology, where $H_0 = 71 \text{ km s}^{-1} \text{ Mpc}^{-1}$, $\Omega_m = 0.3$, and $\Omega_\Lambda = 0.7$ (Spergel et al. 2003).

2. Data

In this section we describe the Smithsonian Hectospec Lensing Survey data set (SHELS). We give an overview of the data set in §2.1. We describe the photometric measurements in §2.2, and the spectroscopic measurements in §2.3, including the $H\alpha$ specific star formation rate in §2.3.1, and aperture effects in §2.3.2.

2.1. Smithsonian Hectospec Lensing Survey

The SHELS magnitude-limited redshift survey includes 9,825 galaxies with total R -band magnitude $R < 20.3$. The galaxies are selected from the Deep Lens Survey F2 field R -band images (DLS; Wittman et al. 2002, 2006). We obtained spectroscopy using Hectospec (Fabricant et al. 2005) at the MMT. The spectroscopic sample is 97.7% complete to $R=20.3$, and the differential completeness at the magnitude limit is 94.6%.

We restrict our analysis to the 6,935 galaxies with redshift $z = 0.080 - 0.376$. The lower redshift limit minimizes aperture effects (§2.3.2) and the upper limit allows measurement of the $H\alpha$ flux (§2.3).

The DLS F2 field covers 4 deg² on the sky centered on R.A. = 9^h19^m32^s.4, decl.=+30°00′00″ (J2000). The Sloan Digital Sky Survey (SDSS; Adelman-McCarthy et al. 2006) also covers this region.

The DLS images come from the Kitt Peak Mayall 4-meter telescope with the Mosaic prime-focus imager (Muller et al. 1998). The DLS observed in the R -band during nights with seeing $\leq 0''.9$. The 1- σ limiting surface brightness in R -band is 29 mag arcsec⁻². The DLS also observed in V -band.

The 0''.9 resolution of the DLS R -band images allows identification of close pairs or merging galaxies with minimum separations of 15 – 20 kpc up to $z \leq 0.3$. The median seeing for the SDSS photometry is 1''.4 PSF in r -band (Adelman-McCarthy et al. 2006). Thus some systems that cannot be distinguished in the SDSS data can be identified in the DLS. A total of eight pairs in the DLS are missing from SDSS.

Objects with stellar light profiles, i.e. AGN at high redshift, may be preferentially excluded

from our sample because DLS objects with stellar light profiles are not targeted for spectroscopy. However, with the DLS 29 mag arcsec⁻² surface brightness limit and the 0".9 resolution, we should be able to detect bright host galaxy bulges to the limiting $z = 0.376$. We discuss AGN detection in more detail in §4.1.

The Hectospec observations identify a spectroscopic pair of emission line galaxies at R.A. = 9^h16^m58^s903, decl. = +29°43'10".597 (J2000). The image, which shows a double-nuclei extended object, and the spectra are available on our website¹. We do not include this object in our analysis because the selection of spectroscopic pairs is not complete or uniform.

Only 230 galaxies in our sample lack spectra (2.3%). Of these, ~ 24 galaxies (10%) may be members of pairs that satisfy our criteria for analysis (§3). The fraction of galaxies in pairs in our sample as a whole is $\sim 10\%$ (§3).

2.2. Photometric measurements

Image processing for the DLS uses the IRAF package MSCRED to correct for bias, to flat field, and to obtain basic astrometric calibration. Wittman et al. (2006) construct a stacked DLS image of each subfield in the R -band, correcting for cosmic rays and saturated objects, fixing the astrometric calibration, and correcting the image shape and photometry for optical distortion. The uncertainty in the R -band magnitude is ~ 0.05 mag. We derive the galaxy catalog using SExtractor (Bertin & Arnouts 1996) on the final stacked images. We remove objects within the radius of the diffraction pattern around bright stars. The total area excluded around 778 stars is 0.215 deg² (5.4% of the survey).

The absolute magnitude M_R calculation includes both k- and evolutionary (e) corrections. We use the k+e correction determined by Annis (2001) using the Pegase code (Le Borgne & Rocca-Volmerange 2002). The k+e correction requires classification as one of nine galaxy types (bright cluster galaxy, elliptical, S0, Sa, Sb, Sbc, Sc, Sd, and irregular). We classify the galaxies according to the SDSS ($g - i$) color and galaxy redshift. We apply the SDSS r -band k+e correction to the DLS R -band

photometry because the shape of the filter band passes are similar and the difference in corrections for the different bands is negligible. We estimate the uncertainty in the k+e correction from the difference in the correction for adjacent galaxy types. The uncertainty ranges from a maximum of ~ 0.02 mag at $z = 0.08$ to 0.03 – 0.13 mag at $z = 0.38$, depending on the galaxy type.

There are 51 galaxies in our $z = 0.080 - 0.376$ sample with a Hectospec redshift but no SDSS photometry for galaxy classification and k+e correction, including three galaxies in major pairs (§3.2). In 34 of the 51 cases, we use the DLS ($V - R$) color to estimate the ($g - i$) color for the k+e correction. For the 17 cases where we lack both DLS ($V - R$) and SDSS data (including two in major pairs), we assume the galaxy type is Sa. The k+e correction for the galaxy type Sa is in the middle of the range for the different galaxy types; choosing a different k+e correction has no significant effect on the results. At the redshift $z = 0.3$, the apparent $R = 20.3$ limit corresponds to a k+e corrected absolute magnitude $M_R = -21.4$ for a typical late-type galaxy, and to $M_R = -21.8$ for a typical early-type galaxy.

2.3. Spectroscopic Measurements

The Hectospec spectrograph 270 line mm⁻¹ grating yields $\sim 6 \text{ \AA pixel}^{-1}$ dispersion over the wavelength range 3700-9300 \AA (Fabricant et al. 2008). The 300 optical fibers with 1".5 diameter are placed radially within a 1° diameter field. About 30 of the fibers measure sky background during each pointing.

We reduce Hectospec data with the standard Harvard-Smithsonian Center for Astrophysics Hectospec reduction pipeline² (Fabricant et al. 2005; Mink et al. 2007). We measure the galaxy redshift using the program RVSAO (Kurtz & Mink 1998; Fabricant et al. 2005). The total RMS internal error in the redshift is 34 km/s for emission line galaxies and 65 km/s for absorption line galaxies, based on repeat observations of 812 emission lines and 542 absorption line galaxies. We further process spectra to correct for atmospheric extinction and to remove the narrow absorption lines from H₂O and O₂ at wavelengths longer than $\sim 6000 \text{ \AA}$.

¹<http://tdc-www.cfa.harvard.edu/instruments/hectospec/progs/tsf/>²<http://tdc-www.harvard.edu/instruments/hectospec/reduce.html>

We also correct for relative throughput as a function of wavelength (Fabricant et al. 2008).

We compute the emission line flux by integrating the counts in a fixed-width band in the rest-frame centered on the central wavelength of the line; we subtract the continuum level. The spectral regions where we measure $H\alpha$ and $H\beta$ emission are $6562.8 \pm 8 \text{ \AA}$ and $4861.3 \pm 8 \text{ \AA}$, respectively. We compute the continuum from the average of regions on either side of the band after rejecting noisy data. The RMS scatter in the line flux is 23% for $H\alpha$, and internal systematic error in $H\alpha$ is $\sim 18\%$, based on duplicate observations of 592 galaxies.

The calibrated R -band photometry from the DLS in a $1''.5$ diameter aperture serves as reference for conversion of counts to flux in the $1''.5$ diameter fiber. This calibration process removes variation caused by seeing, clouds, telescope tracking and guiding, and astrometry and alignment errors for light losses that are wavelength independent (Fabricant et al. 2008).

Comparison of Hectospec spectra with a sample of overlapping SDSS spectra shows that the median ratio of the spectra is constant to $\sim 5\%$ over the range $3850 - 8000 \text{ \AA}$, and the offsets in the ratios of the median $H\alpha$ flux and median rest-frame $H\alpha$ equivalent width ($EW(H\alpha)$) are $\sim 3\%$ (Fabricant et al. 2008).

We also compute the spectroscopic indicator D_n4000 , a measure of the stellar population age, which is defined as the ratio of flux in the band $4000-4100 \text{ \AA}$ to flux in $3850-3950 \text{ \AA}$ (Balogh et al. 1999). The RMS scatter in D_n4000 is 0.086. The internal systematic errors in D_n4000 are very small, 4.5%, based on repeat measurements of 1468 galaxies. The comparison of our measured D_n4000 with an overlapping sample of SDSS spectra shows a median ratio of 1.00 (Fabricant et al. 2008).

2.3.1. $H\alpha$ specific star formation rate

We compute the $H\alpha$ specific star formation rate ($SSFR_{H\alpha}$) from the $H\alpha$ flux ($f_{H\alpha}$) normalized by the R -band $1''.5$ aperture magnitude. The $H\alpha$ flux must first be corrected for stellar absorption and for reddening.

To determine the stellar absorption at $H\alpha$ and $H\beta$, we fit the individual spectrum using

the Tremonti et al. (2004) continuum subtraction method (see also Westra et al. 2010). This method fits the calibrated spectra with stellar population models to estimate the ages of the stellar populations within the galaxy. Like Tremonti et al., we assume that the star formation history of a galaxy can be represented as the sum of discrete bursts of star formation, and we fit for the burst ages.

Figure 1 illustrates the fit of the contributions from the different starburst populations in an example galaxy spectrum. The template spectra that we use are Bruzual & Charlot (2003) stellar population models. The models include 10 different ages of bursts (0.005, 0.025, 0.1, 0.3, 0.6, 0.9, 1.4, 2.5, 5 and 10 Gyr) at Solar metallicity. We also add reddening as an additional parameter using the Charlot & Fall (2000) attenuation model. Finally, we match the models in redshift, pixel size, and spectral resolution to each galaxy spectrum. The core of the code adapted from Tremonti et al. uses the IDL `mpfitfun` routine from the Markwardt library (Markwardt 2009) to find the best fitting combination of models.

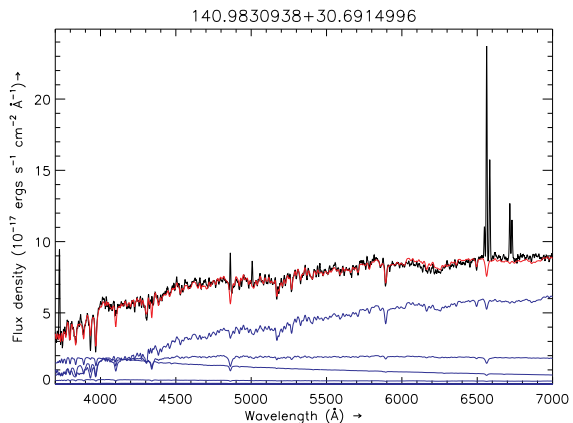


Fig. 1.— An example rest-frame spectrum illustrating the contribution of different stellar populations to the continuum galaxy spectrum. The solid black line is the observed galaxy spectrum. The solid red line shows the modeled galaxy continuum from the sum of the discrete starburst populations, shown as dashed and dash-dot lines (blue).

The absorption-corrected H α flux is:

$$f_{c,H\alpha} = f_{H\alpha} \left(\frac{EW(H\alpha) + EW_{Abs}}{EW(H\alpha)} \right), \quad (1)$$

and similarly for $f_c(H\beta)$. The ratio of f_c/f is equivalent to EW_c/EW . All EW and line fluxes of H α or H β in this paper are absorption corrected.

We correct the H α flux for reddening according to the standard method (Calzetti et al. 2000). We compute the wavelength dependent extinction, A_λ , where the factors $k(H\alpha) = 3.326$ and $k(H\beta) = 4.598$ give the differential extinction between the wavelengths of H α and H β for the case of a starburst galaxy ($k(V) = 4.05$, Calzetti et al. 2000). The parameter $R_{\alpha\beta}$ relates the observed to intrinsic Balmer decrement (2.87; Calzetti 2001).

We correct for reddening using average $E(B - V)$ values for bins of absolute luminosity and redshift. This procedure mitigates the effects of noisy individual H β measurements, which contribute significant noise to the $E(B - V)$ values. Figure 2 shows the EW(H α) versus Balmer decrement for individual galaxies. A population of galaxies with EW(H α) < 20 Å and Balmer decrement > 10 result from noisy H β measurements. The total internal error in EW(H α) is 18% and the error in the Balmer decrement is 25%. We determine the Balmer decrement for each luminosity and redshift bin from the median value in the appropriate bin derived from the 484 galaxies with S/N ≥ 3 in H α , S/N ≥ 2 in H β , EW(H α) > 3 Å, EW(H β) > 2 Å, $D_n4000 \leq 1.44$, and classified as starforming (§4.1). Using the median $E(B - V)$ value eliminates huge and unphysical reddening correction factors for individual galaxies.

Once we correct the H α flux for stellar absorption and for reddening, we calculate the H α luminosity ($L_{H\alpha}$) using the luminosity distance. We convert from $L_{H\alpha}$ to star formation rate using the conversion factor of Kennicutt (1998):

$$SFR_{H\alpha}(M_\odot \text{ yr}^{-1}) = \frac{L_{H\alpha}}{1.27 \times 10^{41} \text{ erg s}^{-1}}. \quad (2)$$

We normalize the H α star formation rate by the galaxy R -band aperture magnitude to compute the H α specific star formation rate (SSFR $_{H\alpha}$). We use the 1''.5 diameter R -band aperture magnitude from the DLS to match the fiber diameter where the H α flux is measured. Thus, no correction for

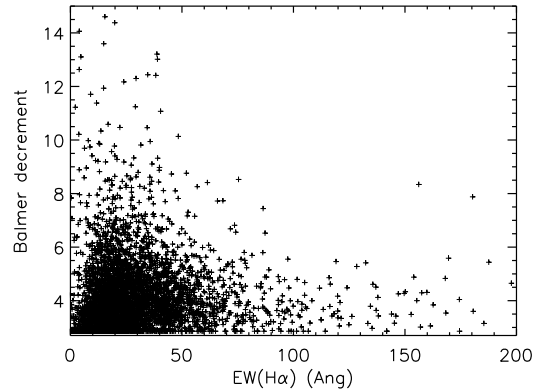


Fig. 2.— EW(H α) versus Balmer decrement for all emission line galaxies. The galaxies with EW(H α) < 20 Å and Balmer decrement > 10 result from noisy H β measurements. We use the median Balmer decrement in bins of absolute luminosity and redshift. We set all Balmer decrement < 2.86 to that value. Measurement uncertainty in EW(H α) is 18% and the uncertainty in the Balmer decrement is 25%.

aperture covering fraction is needed. The normalization factor assumes $1M_\odot = 1L_\odot$ in the R -band and $M_{R(\odot)} = 4.42$ (Binney & Merrifield 1998).

The uncertainty in the SSFR $_{H\alpha}$ follows from the 23% RMS error in the H α flux and the 0.05 mag uncertainty in the normalization. The absorption and reddening corrections contribute additional uncertainty of $\sim 20\%$. We add these contributions to the error in quadrature to estimate a total uncertainty of $\sim 30\%$ in estimates of SSFR $_{H\alpha}$.

2.3.2. Aperture effects

The 1''.5 Hectospec aperture implies that the aperture covering fraction varies as a function of galaxy luminosity and redshift. Kewley et al. (2005) suggest that aperture covering fractions greater than 20% yield star formation rates representative of the galaxy as a whole. The aperture size required to meet this standard varies with both redshift and absolute luminosity because brighter galaxies are generally larger (Kewley et al. 2005). In the volume-limited sample (defined in §3.2), the galaxy radius included

in the fiber varies from $r = 1.1$ kpc at the lower redshift limit ($z = 0.080$) to $r = 3.4$ kpc at the upper redshift limit of the volume-limited sample ($z = 0.310$).

We compute the covering fraction from the difference between the $1''.5$ aperture magnitude and the total galaxy magnitude. Most galaxies in the sample have a covering fraction $> 20\%$; Figure 3 shows the fraction of galaxies with covering fraction $> 20\%$ as a function of redshift for the galaxies (both paired and unpaired) at $z = 0.080 - 0.376$.

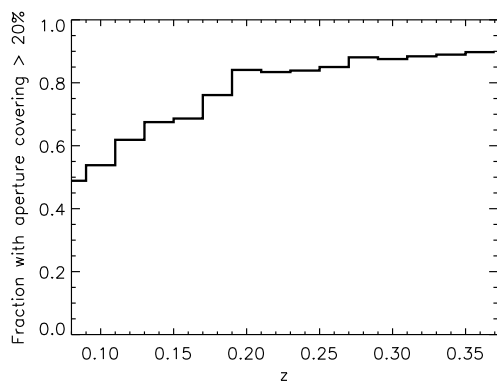


Fig. 3.— The fraction of galaxies where the $1''.5$ aperture includes $> 20\%$ of the galaxy light.

Fabricant et al. (2008) conduct a detailed investigation of aperture effects in their sample of overlapping Hectospec and SDSS spectra, a subset of our full spectroscopic survey. SDSS spectra are acquired through a $3''$ aperture. Thus Fabricant et al. scale the Hectospec line fluxes by the $3''$ aperture DLS R -band magnitude to make direct comparisons with the SDSS line fluxes. They conclude that the median [O II] 3727 \AA and $H\alpha$ line fluxes from Hectospec agree to within $3 - 4\%$ of the SDSS values, and that the scatter in the line fluxes is dominated by systematic uncertainties. The $3 - 4\%$ difference between Hectospec and SDSS line flux measurements is small compared to the 23% RMS scatter in the $H\alpha$ line flux from Hectospec.

The agreement between the Hectospec and SDSS data implies that the $H\alpha$ star formation rate within apertures of 1.5 and $3''$ scale with the R -band galaxy luminosity. The relative agree-

ment between the scaled Hectospec and SDSS $H\alpha$ line flux is independent of the absolute magnitude (see Figure 13 in Fabricant et al. 2008), apparent magnitude, redshift, and 25% light radius of the galaxies. Westra et al. (2009, in prep.) similarly find that the $H\alpha$ luminosity determined from the $1''.5$ fiber and R -band magnitude is consistent with the $H\alpha$ luminosity from the $3''$ aperture photometry and R -band magnitude of Shioya et al. (2008).

Like the $H\alpha$ luminosity, we assume that D_n4000 observed in the $1''.5$ aperture represents the galaxy as a whole. Fabricant et al. (2008) show that the Hectospec and SDSS measurement of D_n4000 agree very well over the scales observed (1.4 to 2.8 kpc radius at $z = 0.1$). This agreement again suggests that measurement of D_n4000 for the stellar population included in the Hectospec aperture is not significantly affected by systematic biases compared to the population observed in the larger SDSS aperture.

3. Pair and Field Sample Selection

We measure the effects of galaxy interactions on the star formation activity and other galaxy properties at intermediate redshift. We use two pair samples derived from the 6,935 galaxies with spectroscopy and $R < 20.3$ in the redshift range $z = 0.080 - 0.376$.

The first sample, the “full” major pairs sample, includes all galaxies in major pairs that meet our projected spatial and line-of sight peculiar velocity criteria (§3.1) in the range $z = 0.080 - 0.376$. There are 622 galaxies in the full major pairs sample.

The second sample, the “volume-limited” major pairs sample, is a subset of the full major pairs sample, and is restricted to galaxies that meet both redshift and absolute luminosity selection criteria (§3.2). The volume-limited major pairs sample allows us to study the strength, frequency, and timescale of triggered star formation. The volume-limited major pairs sample is well suited to comparison with the predictions of the numerical simulations of Di Matteo et al. (2008), who measure the intensity, frequency, and duration of merger-driven star formation in their large suites of numerical simulations of major interactions. The volume-limited major pairs sample contains 339 galaxies.

Our pair samples are the largest spectroscopic samples of pairs to date at intermediate redshift ($z \sim 0.1 - 0.4$). In comparison, the Millennium Galaxy Catalog (MGC; Liske et al. 2003; Driver et al. 2005; Allen et al. 2006) is a 96% complete spectroscopic survey of 10,095 galaxies to $B_{MGC} < 20$ mag. The MGC is similar in number and completeness to our sample but is at lower redshift. De Propris et al. (2007) study pair galaxies in the MGC: they identify a volume-limited sample of 3,237 galaxies in the range $0.010 < z < 0.123$, including 112 galaxies in pairs with projected separation $\Delta D < 28$ kpc [$20 h_{100}^{-1}$ kpc]. The CNOC2 Redshift Survey contains redshifts for $\sim 5,000$ galaxies at $0.1 < z < 0.6$ with a cumulative completeness of 50% and differential completeness of 20% at the limit $R_c \leq 21.5$ (Yee et al. 2000; Patton et al. 2002). Patton et al. (2005) study properties of dynamically close pairs in the CNOC2 survey. Our sample covers the same redshift range but is substantially more complete than CNOC2. Table 1 lists the selection criteria and the number of galaxies in the full major pair sample and in the volume-limited major pair sample.

3.1. Full major pairs sample

We select galaxy pairs with projected spatial separation $\Delta D \leq 70$ kpc, corresponding to the limit $\Delta D \leq 50 h_{100}^{-1}$ kpc commonly applied in previous studies (e.g. Barton et al. 2000). We require a line-of-sight peculiar velocity difference $\Delta V / (1 + z) < 500$ km s $^{-1}$. The limit of $\Delta D \leq 70$ kpc includes pair galaxies with the most significantly enhanced EW(H α) (e.g Barton et al. 2000), while minimizing the presence of interlopers. The ΔV limit is motivated by Barton et al. (2000), who find no significantly enhanced EW(H α) emission in pairs with $\Delta V \gtrsim 500$ km s $^{-1}$ (their Fig. 2b) in their sample of 786 galaxies from the CfA2 Redshift Survey, and is consistent with previous pair studies (De Propris et al. 2007; Woods et al. 2006).

We exclude potential pair galaxies from our sample if either member of the pair lies within a projected 70 kpc from the survey boundary or the edge of the region excluded around a bright star. For galaxies in a compact group, we compare each galaxy to its nearest neighbor; odd numbers of “pair” galaxies can occur in compact groups.

We compute the total pair fraction for all pairs – major and minor – in the redshift interval $z = 0.080 - 0.376$. There are 809 galaxies in major or minor pairs or compact groups that meet the projected spatial and peculiar velocity requirements. The total pair fraction is 12% (809/6,935).

We restrict our sample to major pairs with $|\Delta M_R| < 1.75$, corresponding to a luminosity (approximate mass) ratio $> 1/5$. Simulations of interacting galaxies predict that major interactions are more effective than minor interactions at triggering star formation; only the fainter companion in a minor interaction occasionally shows triggered star formation (Cox et al. 2008). Observations of major and minor pair galaxies support this predicted behavior (Dasyra et al. 2006; Woods & Geller 2007; Ellison et al. 2008; Westra et al. 2009, in preparation.) The full major pair sample includes 622 galaxies in major pairs in the range $z = 0.080 - 0.376$. Figure 4 shows the redshift distribution and Figure 5 shows the distribution of projected separation for the full major pairs sample. Table 2 lists the full major pair sample galaxies and their properties.

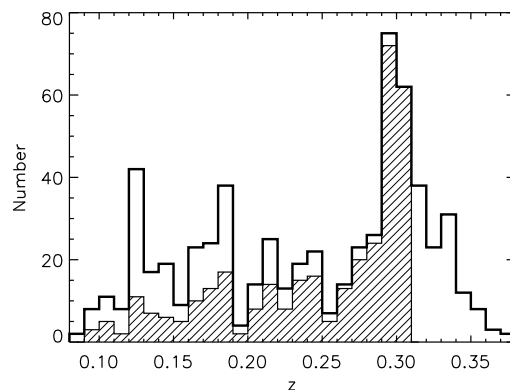


Fig. 4.— Redshift distribution for the full major pair galaxies (open) and for the volume-limited major pair galaxies (filled).

Visible evidence of tidal interactions in the DLS combined BVR -band images, such as tidal tails, marked asymmetries, or extended halos, can be seen in $\sim 1/4$ of the major pair galaxies. Analyzing the morphological features in detail is beyond the scope of this project. The images are available

TABLE 1
CRITERIA AND SIZE OF GALAXY PAIR SAMPLES.

Criteria	Full sample	Volume-limited sample
Major pairs ^a	622	339
Non-AGN ^b	601	324
$D_n4000 < 1.44^c$	302	134
$N_c \leq 4^d$	214	72

Note.— The sample size includes galaxies that meet listed condition and all previously listed conditions.

^a $|\Delta M_R| < 1.75$.

^bAGN classification in §4.1.

^c D_n4000 classification in §4.2.

^d Local density measure N_c described in §5.

TABLE 2
SAMPLE OF MAJOR GALAXY PAIRS^{a,b}

Pair	RA ^c	Dec ^c	z^d	m_R^d	$M_R^{d,e}$	ΔD (kpc)	ΔV^d (km s ⁻¹)	D_n4000^d	SSFR $_{H\alpha}^d$ (M _⊙ yr ⁻¹ /10 ¹⁰ M _⊙)
001	9:14:52.622	30:05:40.858	0.26472	19.56	-21.23	68	388	1.29	1.36
001	9:14:53.920	30:05:40.377	0.26309	19.97	-20.76	68	388	1.79	0.10
002	9:14:52.849	30:17:05.567	0.12805	20.10	-18.80	50	51	0.96	1.26
002	9:14:53.528	30:17:25.933	0.12813	19.17	-19.74	50	51	1.05	3.99
003	9:14:53.583	30:31:44.906	0.25643	20.20	-20.40	65	108	1.14	1.18
003	9:14:54.188	30:31:30.369	0.25688	19.60	-21.14	65	108	0.00	0.04
004	9:14:57.683	29:57:15.864	0.24721	19.08	-21.44	26	133	1.07	3.83
004	9:14:58.198	29:57:15.988	0.24780	19.21	-21.34	26	133	1.11	3.79
005	9:14:57.762	29:49:34.947	0.18074	18.58	-21.20	26	171	1.44	0.36
005	9:14:58.434	29:49:34.583	0.18014	17.81	-22.01	26	171	1.73	0.00

^aFull table available online: <http://tdc-www.cfa.harvard.edu/instruments/hectospec/progs/tsf/>.

^bStandard Λ CDM cosmology: $H_0 = 71$ km s⁻¹ Mpc⁻¹, $\Omega_m = 0.3$, and $\Omega_\Lambda = 0.7$.

^cJ2000 coordinates.

^dTypical error estimates:

cz : 34 km s⁻¹ emission line galaxies, 65 km s⁻¹ absorption line galaxies (§2.3),

m_R : 0.05 mag (§2.2),

D_n4000 : 4.5% (§2.3),

M_R : ~ 0.1 mag, varies with redshift and galaxy type (§2.2),

SSFR $_{H\alpha}$: 30% (§2.3.1).

^ek+e corrected.

on our website¹.

3.2. Volume-limited major pairs sample

We construct a volume-limited sample of major galaxy pairs to study trends in triggered star formation and other galaxy properties. The volume-limited sample contains galaxies in the redshift range $0.080 < z < 0.310$ and with magnitude $M_R < -20.8$. The limits on M_R and z maximize the number of galaxy pairs in the volume-limited sample. The lower redshift limit, $z = 0.080$, minimizes aperture effects (§2.3.2). There are 339 galaxies in major pairs in the volume-limited sample.

The distribution of projected separations (Figure 5) is relatively flat from $15 < \Delta D < 70$ kpc, as expected from the galaxy correlation function (e.g. Estrada et al. 2008). At separations < 15 kpc, galaxies in the DLS images may not be resolved into separate systems. Figure 6 shows the distribution of absolute magnitudes of galaxies in the full major pair sample and in the volume-limited major pair sample.

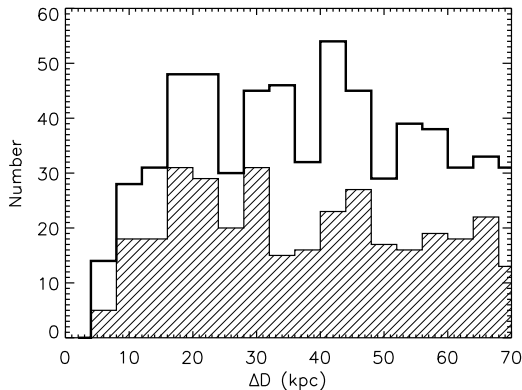


Fig. 5.— Distributions of projected separation for galaxies in the full major pair sample (open) and for the volume-limited major pair sample (filled). The distribution is nearly flat from $10 < \Delta D < 70$ kpc, as expected. At very small ΔD , not all pairs are resolved.

3.2.1. Volume-limited unpaired field sample

We construct a volume-limited sample of galaxies with no detected companions (the “field” sam-

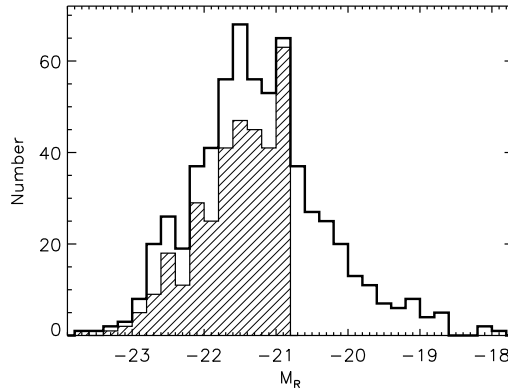


Fig. 6.— Absolute magnitude distribution for galaxies in the full major pair sample (open) and the volume-limited major pair sample (filled).

ple) for comparison with the volume-limited pair sample. The field sample includes only galaxies without companions that satisfy the pair selection criteria. The field galaxies in the volume-limited sample meet the same magnitude ($M_R < -20.8$) and redshift ($z = 0.080 - 0.310$) requirements as the major pair galaxies. The range of magnitude differences excluded from the field galaxies ($|\Delta M_R| < 2$) is slightly broader than the range accepted for major pairs ($|\Delta M_R| < 1.75$) to exclude systems that could marginally be considered major pairs. We exclude galaxies within 70 kpc from the survey boundary or 70 kpc from the boundaries around bright stars. The volume-limited field sample includes 2,234 galaxies.

The distributions of M_R in the volume-limited major pair sample and volume-limited field sample are similar. We use the Kolmogorov-Smirnov (K-S) test to determine that the two distributions are drawn from the sample parent sample ($P_{KS} = 0.37$). The volume-limited major pair sample and the unpaired field sample also have similar distributions of redshifts ($P_{KS} = 0.29$). Figure 7 shows the redshift distribution of field galaxies.

Some of the field galaxies may have a major companion fainter than the survey limit. We estimate the fraction of field galaxies likely to have an undetected major companion. The fraction of galaxies in pairs in the volume-limited sample

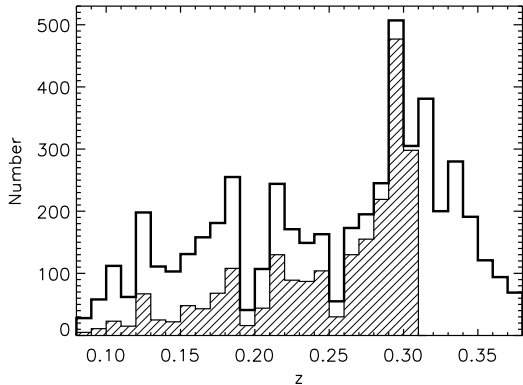


Fig. 7.— Redshift distribution for the field galaxies (open) and the volume-limited field galaxies (filled).

and with apparent magnitude $m_R < 18.55$ is 11% (102/902). The $m_R < 18.55$ limit allows identification of pair galaxies with companions fainter by up to 1.75 mag. There are 1633 out of 2220 field galaxies (74%) in the range $18.55 < m_R < 20.3$ that could have a major companion fainter than our survey limit. An additional factor of 0.5 accounts for a pair galaxy having a 50% probability of being brighter than its companion. Hence the fraction of field galaxies likely to have an undetected major companion is $\sim 4\%$. There are also some field galaxies in later stages of merging such that a companion is unresolved. Because the field sample contains some pairs and merger remnants, any differences in galaxy properties between the pairs and field samples attributable to interactions are lower limits.

4. Spectroscopic Identifiers

In this section we describe galaxy classification metrics to identify candidates for tidally triggered star formation. We identify the galaxies with strong AGN to remove them from our sample of star-forming galaxies (§4.1). We describe the use of the spectroscopic indicator D_n4000 as a galaxy classification tool (§4.2).

4.1. Identification of AGN

We exclude strong AGN from our analysis because measurements of emission lines, such as $H\alpha$, would not accurately represent star formation activity in galaxies with active nuclei. We distinguish narrow-line AGN from star forming galaxies with measurements of the emission lines $H\alpha$, $H\beta$, $[N II]$, and $[O III]$ using the classification metric of Kewley et al. (2006), based on the “BPT” diagrams of Baldwin et al. (1981). The line fluxes $H\alpha$ and $H\beta$ are stellar absorption corrected.

The requirements we place on the spectra for classification are very mild: $EW(H\alpha) > 2 \text{ \AA}$ and $EW(H\beta) > 2 \text{ \AA}$. We impose no requirement on $[N II]$ or $[O III]$ because galaxies without measurable $[N II]$ or $[O III]$ could only have a very weak AGN. Furthermore, galaxies with $EW(H\alpha) < 2 \text{ \AA}$ have minimal star formation. Figure 8 shows the classification diagram for the pair galaxies.

We include composite galaxies in our pair and field samples, but exclude the galaxies classified as AGN. Although these criteria may admit weak AGNs, most of the contribution to the $H\alpha$ emission should be from star-forming regions. There are 119 narrow-line AGNs in the $z = 0.080 - 0.376$ sample, 19 of which are in major pairs (§3.2).

Our ability to detect narrow-line AGN within the host galaxy declines with redshift because the covering fraction of the spectroscopic fiber increases with redshift. At redshift $z = 0.080$, the $1''.5$ fiber diameter corresponds to 2.2 kpc, and at $z = 0.310$, the $1''.5$ fiber covers 6.8 kpc. We also admit fewer AGN at higher redshift into our spectroscopic sample because objects with stellar light profiles are excluded from our spectroscopic catalog.

Despite these caveats to our ability to detect narrow-line AGN at higher redshift, the mean redshift of the narrow-line AGN in the full spectroscopic sample (both pair and unpaired galaxies) is higher than that of the objects classified as starforming or composite: mean $z = 0.27$ and $z = 0.23$, respectively. The redshift distributions differ significantly ($P_{KS} = 1.6 \times 10^{-5}$). We attribute this trend to the evolutionary decline in AGN activity at low redshift (e.g. Brand et al. 2005; Cavaliere 2000).

We identify galaxies with broad emission lines by visually inspecting all spectra that are potential

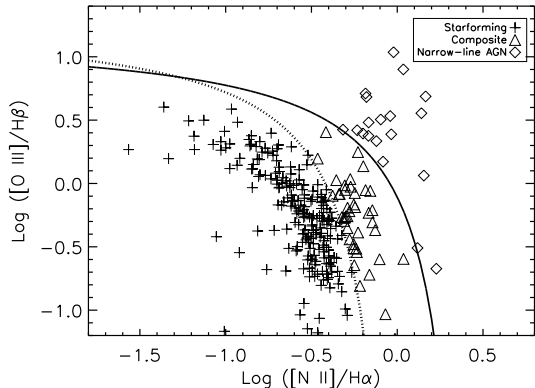


Fig. 8.— Classification of pair galaxies as star-forming, composite, or narrow-line AGN using the Kewley et al. (2006) criteria. The solid black line shows the boundary between composite galaxies and AGN, and the dotted line shows the boundary between star forming and composite galaxies. We include composite galaxies in our sample for analysis of star formation activity.

broadened line objects. The criteria for broad-line AGN candidates is $\text{EW}(\text{H}\alpha) > 3 \text{ \AA}$ and the line flux in a band widened from $\pm 8 \text{ \AA}$ to $\pm 12 \text{ \AA}$ increases the measured $\text{H}\alpha$ flux by more than 10%, or $\text{EW}([\text{N II}]) > 3 \text{ \AA}$ and the line flux in a band widened from $\pm 8 \text{ \AA}$ to $\pm 12 \text{ \AA}$ increases the measured $[\text{N II}]$ flux by more than 10%. We identify 26 galaxies with broadened lines in the $z = 0.080 - 0.376$ sample. Five of these are in major pairs.

We exclude galaxies classified as AGN from our analysis of star formation activity; we retain the non-AGN companion. Table 3 reports the AGN fraction in each pair sample and in the matching unpaired field sample. The AGN fraction in pairs exceeds that in the matching field sample for each of the subsamples. The increase in AGN fraction for both the full and volume-limited major pair samples is a factor of ~ 2 , a significance of $\sim 2\sigma$. The higher AGN fractions in the volume-limited samples (pair and field) compared to the full samples is consistent with the exclusion of lower luminosity galaxies from the volume-limited sample, which are less likely to contain an AGN.

4.2. Galaxy classification by D_n4000

It is useful to segregate galaxies into two categories: early-type galaxies, which are generally gas-poor and have little or no active star formation, and late-type, which contain more gas and have young stellar populations. The gas-rich systems are potentially susceptible to tidally triggered star formation in major interactions (e.g. Mihos & Hernquist 1996; Tissera et al. 2002; Cox et al. 2006; Di Matteo et al. 2007). Interactions between gas-poor galaxies (“dry mergers”) produce little or no star formation activity, although they contribute substantially to the build-up of massive galaxies (e.g. Tran et al. 2005; Van Dokkum 2005; Cattaneo et al. 2008). Our analysis of star formation activity in pair galaxies focuses on the late-type systems.

There are a number of classification schemes to separate the early and late-type galaxy populations. Photometric discriminants include color, concentration, and absolute magnitude (e.g. Strateva et al. 2001; Kauffmann et al. 2003b), and spectroscopic methods include D_n4000 and $\text{H}\delta$ absorption (Kauffmann et al. 2003a). The D_n4000 indicator discriminates by stellar population age. At wavelengths bluer than 4000 \AA , metal lines in low mass stars absorb the light and cause a “break” in the spectrum. As the stellar population ages and the massive, hot stars die off, D_n4000 increases monotonically with time. Kauffmann et al. (2003a) use stellar population models to show that galaxies with $D_n4000 \lesssim 1.5$ have young stellar populations ($\lesssim 1 \text{ Gyr}$). Metallicity has a strong effect on the value of D_n4000 only after 1 Gyr past a burst of star formation (see Fig. 2 in Kauffmann et al. 2003a). Measurement of D_n4000 is insensitive to galaxy reddening.

Vergani et al. (2008) use D_n4000 to separate spectroscopic early-type galaxies from late-type galaxies at a dividing line of $D_n4000 = 1.5$ in their analysis of galaxy stellar mass assembly in the VIMOS VLT Deep Survey. Mignoli et al. (2005) also use $D4000 = 1.6$ as a dividing line (different definition of $D4000$ from Bruzual 1983: ratio of flux in bands $4050\text{-}4250 \text{ \AA}$ to $3750\text{-}3950 \text{ \AA}$) along with other spectral measurements to classify galaxies in the K20 survey, a near-IR selected redshift survey. We follow this approach.

The distribution of D_n4000 is bimodal, sepa-

TABLE 3
AGN FRACTION

Sample	Pair ^a	Field ^b	Significance	Pair sample size
Full	$8 \pm 2\%$	$4 \pm 2\%$	2σ	280
Volume limited	$12 \pm 3\%$	$5 \pm 2\%$	2σ	128

^aFraction of AGNs compared to fraction of galaxies that meet our criteria for classification (§4.1). We identify only very bright AGNs with our spectra and our classification criteria.

^bProportional representation of field galaxies matching the M_R and redshift distribution of the pair sample.

rating galaxy populations dominated by old stars from systems with recent star formation. Figure 9 shows the distribution of D_n4000 for the 6,644 galaxies (both pair and unpaired) at $z = 0.080 - 0.376$ with a robust D_n4000 measurement. The peaks are at ~ 1.15 and ~ 1.75 . Kauffmann et al. (2003a) similarly observe a bimodal distribution in D_n4000 , with peaks at 1.30 and 1.85 in their sample of $\sim 100,000$ galaxies in the SDSS. We choose the minimum between the bimodal distribution as our dividing line, $D_n4000 = 1.44$ (Figure 9). We refer to galaxies with $D_n4000 \leq 1.44$ as “low” D_n4000 galaxies and those with $D_n4000 > 1.44$ as “high” D_n4000 galaxies. Our analysis of star formation activity includes the low D_n4000 galaxy in a mixed pair, but does not require both galaxies to have $D_n4000 < 1.44$.

The emission line fraction is a strong function of D_n4000 . Figure 10 shows the steep decline in the fraction of emission line galaxies between $D_n4000 = 1.3 - 1.5$. The emission line galaxies have $\text{EW}(\text{H}\alpha) \geq 3$ or $\text{EW}([\text{O II}]) \geq 3$. Thus segregating by D_n4000 is reasonable and corresponds well to segregating by the presence of emission lines.

We also compare the use of D_n4000 for galaxy classification with color, another widely used indicator of galaxy type. Figure 11 shows the bimodal distribution of rest-frame SDSS ($g - r$) color versus D_n4000 . We compute the rest-frame SDSS ($g - r$) color using the k+e correction determined by Annis (2001) from the Pegase code (Le Borgne & Rocca-Volmerange 2002). The sep-

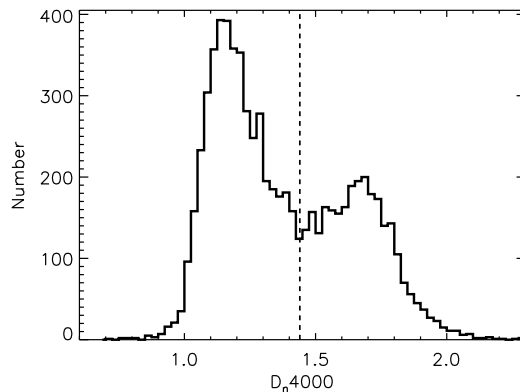


Fig. 9.— Distribution of D_n4000 for all galaxies in the spectroscopic sample. The bimodal distribution has a local minimum at $D_n4000 = 1.44$ (dashed line).

aration by D_n4000 is more sharply defined than that of rest-frame color. The rest-frame galaxy colors are affected by reddening, and depend on the noisy k+e corrections. D_n4000 provides a well-defined method to segregate galaxies and has the advantage that no redshift dependent corrections are required.

5. Local Density Effects

Because pair galaxies are more common in higher density regions (Barton et al. 2007), and because cluster and group galaxies are more likely

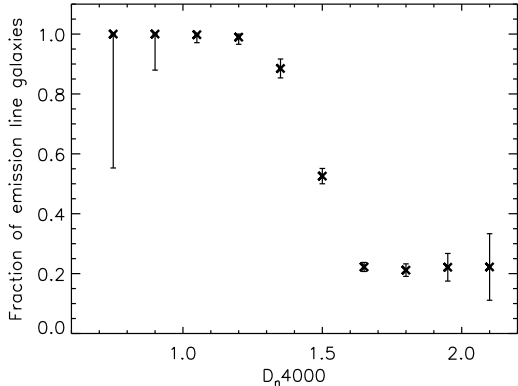


Fig. 10.— Fraction of emission-line galaxies as a function of D_n4000 for all galaxies in the spectroscopic sample, excluding AGN. Emission line galaxies have $\text{EW}(\text{H}\alpha) \geq 3$ or $\text{EW}([\text{O II}]) \geq 3$. There is a steep decline in the fraction between $D_n4000 = 1.3 - 1.5$. Error bars from bootstrap resampling indicate the 95% confidence intervals.

to be red with less active star formation than isolated galaxies (e.g. Hubble & Humason 1931; Cooper et al. 2007; Gerke et al. 2007), comparisons between pair and field populations without attention to density can strongly bias the interpretation of studies of close pairs. Barton et al. (2007) emphasize that including high density regions suppresses the detection of triggered star formation.

To compare the environment of pair and field galaxies, we compute the number of companions (N_c) within a co-moving sphere of radius 985 kpc centered on the galaxy (radius equivalent to $700 h_{100}^{-1} \text{kpc}$). The 985 kpc radius is within the typical virial radius of clusters ($\sim 1 h_{100}^{-1} \text{Mpc}$, Rines et al. 2003), and maximizes the survey area included in our analysis. This density measurement is consistent with that of Barton et al. (2007). We measure N_c within the volume-limited sample, requiring that the galaxy reside within $z = 0.080 - 0.310$ and have magnitude $M_R < -20.8$. We count all neighboring galaxies, not just major companions. We exclude regions within 985 kpc of the survey edge.

Barton et al. (2007) predict that most observed pair galaxies reside in higher mass cluster or

group-sized halos, whereas field galaxies are usually in isolated low mass halos. We test this prediction with our complete volume-limited data set, using N_c as a proxy for halo membership. Note that our N_c counts neighbors; the halo count N in Barton et al. counts total halo occupation, i.e. $N = N_c + 1$.

Figure 12 shows the fraction of galaxies with various N_c as a function of projected distance to the nearest neighbor. Pair galaxies fall in the range $\Delta D < 70 \text{ kpc}$. As Barton et al. show, pairs occur more frequently in locally dense regions. We find that 32% of pair galaxies have $N_c \geq 8$. The overall fraction of galaxies in dense regions is smaller: 19% of all galaxies lie in regions with $N_c \geq 8$.

Our observations are in excellent agreement with the predictions of Barton et al. (2007). They find that 39% of pair galaxies are in a host halo with total number of galaxies $N \geq 9$; 19% of galaxies in the sample as a whole have $N \geq 9$ ($N_c \geq 8$). Selecting a sample of field galaxies for a fair comparison of specific star formation rates thus necessitates consideration of local density effects.

Selecting star forming galaxies with young stellar populations (low D_n4000) already reduces the effects of the environment because young, blue galaxies are relatively more abundant in low density regions. In the volume-limited major pair sample, 63% of the low D_n4000 non-AGN galaxies reside in regions with $N_c \leq 4$.

Restricting the analysis of star formation activity solely by D_n4000 does not, however, eliminate differences in star formation activity with local density. The distribution of local densities differs between low D_n4000 pair and field galaxies ($P_{KS} = 1.6 \times 10^{-5}$). Thus we restrict any direct comparisons of specific star formation activity in pairs and field galaxies to low density regions to ensure that density effects do not dominate our measurements of star formation activity. A moderate limit of $N_c \leq 4$ maximizes our sample size.

6. Measurements of tidally triggered star formation

Here we quantify the frequency, strength, and timescale of the triggered star formation for galaxies at intermediate redshift. We examine trends in star formation activity across redshift and lu-

minosity for the galaxies in the volume-limited sample. The completeness and quality of spectrophotometry enable us to carry out the most detailed spectroscopic analysis of pair galaxies to date in the redshift range $z = 0.080 - 0.376$. We examine the $H\alpha$ specific star formation rate ($SSFR_{H\alpha}$, §2.3.1), the spectroscopic parameter D_n4000 (§4.2), and a set of stellar population models (§2.3.1).

The volume-limited pair sample is well suited to comparison with the predictions of numerical simulations. We compare our observations with the predictions of Di Matteo et al. (2008), who measure the intensity, frequency, and duration of merger-driven star formation in their large suites of numerical simulations of major interactions.

6.1. Star formation indicators and projected separation

We examine a set of star formation indicators as a function of projected separation to look for the signature of triggered star formation at redshifts $0.080 - 0.376$. The star formation - ΔD anti-correlation frequently observed at low redshift (Barton et al. 2000; Lambas et al. 2003; Nikolic et al. 2004; Woods et al. 2006; Geller et al. 2006; Woods & Geller 2007; Li et al. 2008a; Ellison et al. 2008) results from an increase in central star formation activity triggered by a close pass from a neighboring galaxy. As the pair galaxies move apart and the burst ages, the star formation activity decreases.

We observe a strong anti-correlation between $SSFR_{H\alpha}$ and ΔD in the sample of all low D_n4000 major pair galaxies at $z = 0.080 - 0.376$ (at all local densities). The Spearman-rank test computes a probability of no correlation of $P_{SR} = 6.0 \times 10^{-4}$ for the 134 galaxies in the sample (Figure 13, top left panel.) The range of absolute luminosities and local densities in this sample corresponds to that included in typical samples at low redshift (e.g. Barton et al. 2000).

Figure 13 shows the mean $SSFR_{H\alpha}$ as a function of ΔD for low D_n4000 galaxies in low density regions in the volume-limited major pairs sample (top right panel). We measure a correlation between $SSFR_{H\alpha}$ and ΔD for the 70 galaxies in this sample, where $P_{SR} = 1.3 \times 10^{-2}$. The decreased significance compared to the sample of all major

pair galaxies results from the reduction in sample size. Excluding the lowest luminosity galaxies from the volume-limited sample may also reduce the signal of the interaction because low luminosity galaxies are more strongly affected than the more luminous galaxies.

We measure a weak correlation between ΔD and D_n4000 for the low D_n4000 galaxies in the volume-limited pair sample at the level of $P_{SR} = 5.1 \times 10^{-2}$; bursts with small ΔD have small D_n4000 (Figure 13, bottom left panel). This trend is consistent with the expectation that close pairs have had the most recent starbursts, and hence harbor the youngest stellar populations.

We apply another measure of the recent star formation based on the stellar population models. The model-determined fraction of total luminosity at 5500 \AA from the youngest discrete starburst population age (5 Myr) correlates with ΔD for the volume-limited major pair sample: $P_{SR} = 1.4 \times 10^{-2}$. Pairs at the smallest ΔD have the highest fractional contribution from a 5 Myr stellar population, compared to galaxies with larger ΔD (Figure 13, bottom right panel).

These results are consistent with other recent observations. At redshifts of $0.1 < z < 1.1$, Lin et al. (2007) likewise observe an anti-correlation between the median infrared luminosity of merging galaxies and pair separation in their sample of ~ 100 systems with data from the DEEP2 Galaxy Redshift Survey and HST/ACS imaging. de Ravel et al. (2009) similarly find that the galaxy pairs at the smallest separations have the greatest median EW([O II]) in their sample of 251 pairs in the VIMOS VLT Deep Survey (Le Fèvre et al. 2005), which has a mean of redshift of $z = 0.76$.

We next explore properties of the galaxies that drive the correlation between star formation indicators and ΔD — the galaxies with significant star formation rates at small separation. The galaxies with $\Delta D < 25 \text{ kpc}$ and $SSFR_{H\alpha} > 4 M_{\odot} \text{ yr}^{-1}/10^{10} M_{\odot}$ have luminosities similar to the rest of the low D_n4000 galaxies in the volume-limited sample ($M_R \simeq -21.4$). These galaxies are bright; $M_R^* \simeq -22.1$ for all galaxies in our spectroscopic sample in this redshift range (Diaferio et al. 2010, in prep.). The correlation between $SSFR_{H\alpha}$ and ΔD for luminous galaxies at redshifts $z = 0.1 - 0.3$ is an interesting observation

for comparison with lower redshift results.

In the low redshift CfA2 Redshift survey, the lower mass galaxies (measured by rotation velocities) exhibit an anti-correlation between $\text{EW}(\text{H}\alpha)$ and ΔD ; more massive galaxies do not (Barton (1999)). They conclude that the least massive galaxies exhibit the strongest bursts of star formation and are responsible for driving their observed $\text{EW}(\text{H}\alpha)$ - ΔD correlation. Both Woods & Geller (2007) and Ellison et al. (2008) find at low redshift that low mass (luminosity) galaxies exhibit relatively more powerful triggered specific star formation than high mass galaxies.

Finding luminous galaxies with strong evidence of triggered star formation at intermediate redshift is consistent with “downsizing” (Cowie et al. 1996), which suggests that higher mass (luminosity) galaxies formed their stars earlier, and that the lower mass galaxies have more efficient star formation at later times than the higher mass galaxies (Guzman et al. 1997; Brinchmann & Ellis 2000; Kodama et al. 2004; Bell et al. 2005; Juneau et al. 2005; Noeske et al. 2007).

6.2. Frequency and strength of triggered star formation

Gravitational interactions clearly trigger star formation in some cases (see references in §1). Some galaxies fail to have enhanced star formation because the pairs have not yet reached perigalacticon, the pairs may be mere interlopers along the line-of-sight, or they may have internal structure less conducive to gaseous inflows (Mihos & Hernquist 1996).

We place limits on the frequency of triggered star formation by comparing the $\text{SSFR}_{\text{H}\alpha}$ of the low D_n4000 pair galaxies with those of the low D_n4000 unpaired field galaxies in the volume-limited samples. Figure 14 shows the normalized distributions of $\text{SSFR}_{\text{H}\alpha}$ for the low D_n4000 galaxies in major pairs and the unpaired field galaxies. The dotted line indicates the median $\text{SSFR}_{\text{H}\alpha}$ for the field galaxies. Table 4 lists the quartiles of the distribution and the fraction of pair galaxies with $\text{SSFR}_{\text{H}\alpha}$ more than twice the field median. The results for the very close pairs, $\Delta D < 25$ kpc, are listed separately.

Table 4 shows that the low D_n4000 major pair

galaxies have an excess of high $\text{SSFR}_{\text{H}\alpha}$ compared to the low D_n4000 field galaxies. We define the fraction of pair galaxies experiencing enhanced specific star formation as $\text{SSFR}_{\text{H}\alpha} = 2 \times F_{50}$, where F_{50} is the median $\text{SSFR}_{\text{H}\alpha}$ for the field galaxies. According to this definition, $32 \pm 7\%$ of major pair galaxies experience enhanced specific star formation. A greater fraction of close pairs with $\Delta D < 25$ kpc, exhibit enhanced specific star formation rates: $42 \pm 13\%$. Observing a greater fraction of close pairs with enhanced star formation is consistent with triggering at the closest approach and the subsequent decline as the burst ages and the pair moves apart. We find only one galaxy with $\text{SSFR}_{\text{H}\alpha} > 5 \times F_{50}$.

A number of generic selection issues affect the measured frequency and strength of triggered star formation. The first issue is that a small fraction ($< 4\%$) of the field galaxies is likely to be in a pair with an undetected companion (§3.2.1). Second, excluding galaxies with strong AGN preferentially excludes pairs with active star formation because triggered AGN activity and star formation activity often occur as part of the same process (e.g. Hopkins et al. 2008). Third, we are unable to resolve some pairs or mergers at separations $\Delta D < 15$ kpc, where the strongest star formation enhancement is expected (e.g. Barton et al. 2000). Our measurement of the frequency and strength of triggered star formation should therefore be interpreted as lower limits.

We compare measurement of the frequency of triggered star formation from our volume-limited major pairs sample with the predictions of Di Matteo et al. (2008), who use numerical simulations to study the frequency, intensity, and duration of triggered star formation activity. Between 25 and 50% of their “fly-bys” have star formation rates twice the isolated case (see their Table D.1.) We compare with their fly-bys and not their merger scenario because the galaxies in our sample are distinct systems, which have not yet had a final merger. Our results are consistent with the predictions of Di Matteo et al.

One difference between our observations and the Di Matteo et al. simulations is that their maximum star formation rate refers to the lifetime of the galaxy; ours represents a snapshot in time. Because the most intense bursts of star formation occur over relatively short time scales in the course

TABLE 4

DISTRIBUTION OF SPECIFIC STAR FORMATION RATES IN PAIRS AND UNPAIRED FIELD GALAXIES

Sample ^a	Q_{25} ^b	Q_{50}	Q_{75}	$> 2F_{50}$ ^c	Sample size
Pair	1.55	2.61	4.26	$32 \pm 7\%$	72
Close pair ^d	1.87	3.11	4.43	$42 \pm 13\%$	26
Field	1.18	1.80	2.86	$14 \pm 1\%$	777

^aPair and field samples derive from the volume-limited sample of low D_n4000 galaxies, where $M_R < -20.8$. Pair galaxies are in major pairs, $|\Delta M_R| < 1.75$.

^bQuartile of the distribution of $\text{SSFR}_{H\alpha}$ in units of $M_\odot \text{yr}^{-1} / 10^{10} M_\odot$.

^cFraction of pair galaxies with $\text{SSFR}_{H\alpha} > 2F_{50}$, where F_{50} is the median of the field galaxies in the same redshift bin.

^dClose pair: $\Delta D < 25$ kpc.

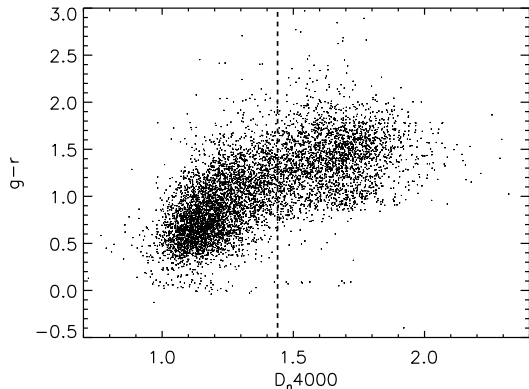


Fig. 11.— D_n4000 versus rest-frame $(g-r)$ color. Two galaxy populations are visible: systems with blue colors (lower left), and systems with red colors (upper right). The dashed line indicates $D_n4000 = 1.44$ (see Figure 9).

of the merger (see Figure 4 in Di Matteo et al.), we are unlikely to observe pair galaxies at maximum intensity. We therefore expect to measure a lower frequency than that predicted by Di Matteo et al. This prediction is consistent with our finding only one galaxy with $\text{SSFR}_{H\alpha} > 5 \times F_{50}$; Di Matteo et al. find that 15% of their major mergers have star formation enhanced by this large factor.

The frequency and strength of triggered star formation that we measure are consistent with the observations of Jogee et al. (2008), who find that the average star formation rate of strongly disturbed galaxies exhibits only a modest increase over the morphologically undisturbed galaxies in their sample of $\sim 4,500$ galaxies at $0.24 < z < 0.80$. Our results are also in line with the low redshift observations of Ellison et al. (2008), who measure star formation rate enhancement in SDSS galaxies at $z < 0.16$. Li et al. (2008a) find that the SDSS systems with the highest star formation rates are likely to have a companion, but not all systems with close companions have high star formation rates.

A consistent explanation for the range of results drawn from simulations and observations is that strongly enhanced star formation is rare and short lived. Simulations can track the maximum enhancement across the lifetime of the merger; dif-

ferent types of pair selection probes systems in different stages of the interaction. Density effects may also reduce the impact of observations of star formation in pairs (Barton et al. 2007).

6.3. Duration of triggered star formation

We use the stellar population models described in §2.3.1 to compare the stellar composition of pair and unpaired field galaxies. The stellar population models fit the spectra with a discrete set of starbursts of age 0.005, 0.025, 0.1, 0.3, 0.6, 0.9, 1.4, 2.5, 5 and 10 Gyr. From the models we extract the contribution of each starburst population to the flux at 5500 Å.

Figure 15 shows the ratio (pair/field) of the mean fraction of flux at 5500 Å attributed to each discrete starburst as a function of starburst age for the starburst populations included in the model. The pair galaxies clearly contain a larger fraction of young stellar populations up to burst ages $\sim 300\text{--}400$ Myr. The ratio of the mean fraction of flux from each starburst population dips slightly below one for burst ages $\gtrsim 500$ Myr, because the younger stellar populations contain a greater fraction of the flux in the pair galaxies.

Our measurement agrees well with the results of Barton et al. (2000), who apply spectral synthesis models (Leitherer et al. 1999; Bruzual & Charlot 1996) to their data from the CfA2 Redshift Survey (Falco et al. 1999). They determine that the H α emission and the galaxy colors are best described by a burst with a continuous duration $\gtrsim 100$ Myr on top of the pre-existing stellar population. The simulations of Di Matteo et al. (2008) similarly suggest a merger-driven starburst duration of up to a few hundred Myr, consistent with our measured duration.

7. Summary and conclusion

We examine spectroscopic properties of pair and field galaxies to quantify effects of gravitational interactions at intermediate redshift. Our sample derives from the Smithsonian Hectospec Lensing Survey (SHELS; Geller et al. 2005, 2010). SHELS includes 9,825 galaxies and is 97.7% spectroscopically complete to $R = 20.3$ over an area of 4 deg². We select for galaxies in the redshift range $z = 0.080 - 0.376$. This survey represents the most complete spectroscopic sample in its red-

shift range.

We focus on the systems that have the potential to exhibit bursts of star formation as a result of the interaction. Substantial evidence shows that major pairs are more strongly affected by the interaction. We identify a full set of major ($|\Delta M_R| < 1.75$) pairs including 622 galaxies in the redshift range $z = 0.080 - 0.376$, and a volume-limited subset of major pairs in the redshift range $z = 0.080 - 0.310$, including 327 galaxies to $M_R = -20.8$.

Within our major pair sample, we further narrow our selection using the spectroscopic index $D_n4000 = 1.44$ as the divide between systems with older stellar populations, and systems with young stellar populations that likely contain gas. We further restrict our sample to systems with low surrounding density, which we measure with a count of neighbors within a volume of comoving radius 985 kpc.

The spectroscopic diagnostics of H α specific star formation rate ($SSFR_{H\alpha}$), D_n4000 , and a set of stellar population models enable the investigation of the strength, frequency, and timescale of triggered star formation. We show:

1. The spectroscopic indicator D_n4000 provides a useful classification metric and corresponds closely with identification of emission line galaxies.
2. The star formation indicators $SSFR_{H\alpha}$, D_n4000 , and presence of young stellar populations exhibit an anti-correlation with ΔD , demonstrating that bursts of star formation are associated with close proximity to a major companion.
3. $32 \pm 7\%$ of major pair galaxies in the volume-limited sample experience enhanced specific star formation activity at twice the median of the unpaired field galaxies. For very close pairs ($\Delta D < 25$ kpc), the fraction is $42 \pm 13\%$. This trend is consistent with the tidal triggering picture.
4. We use stellar population models to show the burst of star formation following an interaction has a duration of $\sim 300 - 400$ Myr. Pair galaxies show an increase over the field in the light fraction from young stellar populations for burst ages up to $\sim 300 - 400$ Myr.

The most effective way to increase our ability to measure differences between pair and field galaxies as a function of redshift, or to determine the AGN fraction in pairs would be to observe a larger population of very close pairs ($\Delta D < 15$ kpc) at redshift $z \sim 0.3$ using small aperture spectroscopy. It is important to have high resolution photometric data in combination with good seeing to distinguish close pairs.

Acknowledgment

This work benefited greatly from discussions with Elizabeth Barton, Nelson Caldwell, Scott Kenyon, and Lisa Kewley. We thank the members of DFW's PhD thesis committee for their comments that improved this work: Lars Hernquist, Robert Kirshner, and Andrew Szentgyorgyi. We thank the anonymous referee for a helpful and knowledgeable report.

We gratefully acknowledge the contribution of the CfA's Telescope Data Center team, especially Doug Mink, Susan Tokarz, and William Wyatt for their work with the Hectospec data reduction pipeline. We thank the Hectospec engineering team, including Robert Fata, Tom Gauron, Edward Hertz, Mark Mueller, and Mark Lacasse, and the instrument specialists Perry Berlind and Michael Calkins, along with the rest of the staff at the MMT Observatory.

Funding for the SDSS and SDSS-II has been provided by the Alfred P. Sloan Foundation, the Participating Institutions, the National Science Foundation, the U.S. Department of Energy, the National Aeronautics and Space Administration, the Japanese Monbukagakusho, the Max Planck Society, and the Higher Education Funding Council for England. The SDSS Web Site is <http://www.sdss.org/>.

Facilities: MMT (Hectospec), Sloan, KPNO:CFT (Mosaic)

REFERENCES

- Adelman-McCarthy, J., Agueros, M. A., Allam, S. S., et al. 2006, *ApJS*, 162, 38
- Allen, P. D., Driver, S. P., Graham, A. W., Cameron, E., Liske, J., De Propis, R. 2006, *MNRAS*, 371, 2
- Alonso, M. S., Tissera, P., Coldwell, G., & Lambas D. G. 2004, *MNRAS* 352, 1081
- Alonso, M. S., Lambas D. G., Tissera, P., & Coldwell, G. 2006, *MNRAS*, 367, 1029
- Alonso, M. S., Lambas D. G., Tissera, P., & Coldwell, G. 2007, *MNRAS* 375, 1017
- Annis, J. 2001. <http://home.fnal.gov/~annis/astrophys/kcorr/kcorr.html>
- Arp, H. 1966, *Atlas of Peculiar Galaxies*. California Inst. of Technology, Pasadena
- Baldwin J. A., Phillips M. M., Terlevich R., 1981, *PASP*, 93, 5
- Balogh M.L., Morris S.L., Yee H.K.C., Carlberg R.G., Ellingson E., 1999, *ApJ*, 527, 54
- Barnes J. E. & Hernquist L. E., 1991, *ApJ*, 370, L65
- Barnes, J. E., & Hernquist, L. 1992, *ARA&A*, 30, 705
- Barthel, P. D. 2006, *A&A*, 458, 107
- Barton, E. J. 1999, Ph.D. Thesis, Harvard University
- Barton, E. J., Geller, M. J., Kenyon, S. J. 2000, 530, 660
- Barton Gillespie, E., Geller, M. J. & Kenyon, S.J. 2003, *ApJ*, 582, 668
- Barton, E. J., Arnold, J. A., Zentner, A. R., Bullock, J. S. & Wechsler, R. H. 2007, *ApJ*, 671, 1538
- Bell E. F. et al., 2005, *ApJ*, 625, 23
- Bergvall, N., Laurikainen, E. & Aalto, S. 2003, *A&A*, 405, 31
- Bertin, E. & Arnouts, S. 1996, *A&AS*, 117, 393
- Best, P. N., Kauffmann, G., Heckman, T. M., Brinchmann, J., Charlot, S., Ivezić, ., & White, S. D. M. 2005, *MNRAS*, 362, 25
- Blanton, M. R. & Roweis, S. 2007, *AJ*, 133, 734
- Binney, J. & Merrifield, M. 1998, *Galactic Astronomy*, Table 2.1, pp. 53

- Brand, K. et al., 2005, *ApJ*, 26, 723
- Brinchmann J., Ellis R. S., 2000, *ApJ*, 536, L77
- Brotherton, M. S., et al. 1999, *ApJ*, 520, L87
- Bruzual, A. G. 1983, *ApJ*, 273, 105
- Bruzual, A. G., & Charlot, S. 1996, AAS CD-ROM Series, Vol. 7, Astrophysics on Disk (Washington, D.C.: AAS)
- Bruzual, G. & Charlot, S. 2003, *MNRAS*, 344, 1000
- Calzetti, D. 2001, *PASP*, 113, 1449
- Calzetti, D., Armus, L., Bohlin, R. C., Kinney, A. L., Koornneef, J., & Storchi-Bergmann, T. 2000, *ApJ*, 533, 682
- Canalizo, G., & Stockton, A. 2001, *ApJ*, 555, 719
- Cardelli, J. A., Clayton, G. C., & Mathis, J. S. 1989, *ApJ*, 345, 245)
- Cattaneo, A., Dekel, A., Faber, S. M., & Guiderdoni, B. 2008, *MNRAS*, submitted (arXiv:0801.1673)
- Cavaliere, A., & Vittorini, V. 2000, *ApJ*, 543, 599
- Charlot, S. & Fall, S. M. 2000, *ApJ*, 539, 718
- Cole, S., Lacey, C. G., Baugh, C. M., Frenk, C. S. 2000, *MNRAS*, 319, 168
- Colless, M. et al. 2001, *MNRAS*, 328, 1039
- Cooper, M. C. et al. 2007, *MNRAS*, 376, 1445
- Cowie L. L., Songaila A., Hu E. M., Cohen J. G., 1996, *AJ*, 112, 839
- Cox, T. J., Jonsson, P., Primack, J. R., Somerville, R. S. 2006, *MNRAS*, 373, 1013
- Cox, T. J., Jonsson, P., Somerville, R. S., Primack, J. R., Dekel, A. 2008, *MNRAS*, 384, 386
- Dahari, O. 1985, *ApJS*, 57, 643
- Dasyra, K. M., Tacconi, L. J., Davies, R. I., Genzel, D. L., Naab, T., Burket, A., Veilleux, S., & Sanders, D. B. 2006, *ApJ*, 638, 745
- De Propris R., Conselice, C. J., Liske, J., Driver, S. P., Patton, D. R., Graham, A. W., Allen, P. D. 2007, *ApJ*, 666, 212
- de Ravel, L. et al. 2009, *A&A*, 498, 379
- Di Matteo, T., Springel, V., & Hernquist, L. 2005, *Nature*, 433, 604
- Di Matteo, P., Combes, F., Melchior, A.-L., Semelin, B. 2007, *A&A*, 468, 61
- Di Matteo, P., Bournaud, F., Martig, M. Combes, F., Melchior, A.-L., Semelin, B. *astro-ph/0809.2592*, Accepted to *A&A*
- Donzelli, C. J. & Pastoriza M. G. 1997, *ApJS*, 111, 181
- Driver, S. P., Liske, J., Cross, N. J. G., De Propris, R., & Allen, P. D. 2005, *MNRAS*, 360, 81
- Ellison, S. L., Patton, D. R., Simard, L. & McConnell, A. W. 2008, *AJ*, 135, 1877
- Estrada, J., Sefusatti, E., Frieman, J. A. 2009, *ApJ*, 692, 265
- Fabricant, D. G. et al. 2005, *PASP*, 117, 1411
- Fabricant, D. G., Kurtz, M. J., Geller, M. J., Caldwell, N., Woods, D. 2008, *PASP*, 120, 1222
- Falco, E. et al. 1999, *PASP*, 111, 438
- Geller, M. J., Dell'Antonio, I. P., Kurtz, M. J., Ramella, M., Fabricant, D. G., Caldwell, N., Tyson, J. A., & Wittman, D. 2005, *ApJ*, 635, L125
- Geller, M. J. Kenyon, S. J., Barton, E. J., Jarret, T. H., Kewley, L. J. 2006, *AJ*, 132, 2243
- Geller, M. J., Kurtz, M. J., Dell'Antonio, I., Ramella, M. & Fabricant, D. 2010, *ApJ*, in press
- Gerke, B. F. et al. 2007, *MNRAS*, 376, 1425
- Guzman R., Gallego J., Koo D. C., Phillips A. C., Lowenthal J. D., Faber S. M., Illingworth G. D., Vogt N. P., 1997, *ApJ*, 489, 559
- Hawkins, E. et al. 2003, *MNRAS*, 346, 78
- Hennawi, J. F., et al. 2006, *AJ*, 131, 1
- Hernquist, L. & Mihos, J. C. 1995, *ApJ*, 448, 41
- Hopkins, P. F., Hernquist, L., Cox, T. J., Robertson, B., & Springel, V. 2006, *ApJS*, 163, 50

- Hopkins, P. F., Hernquist, L., Cox, T. J., & Kereš, D. 2008c, *ApJS*, 175, 356
- Hubble, E. & Humason, M. L. 1931, *ApJ*, 74, 43
- Hummel, E. 1981, *A&A*, 96, 111
- Jahnke, K., Kuhlbrodt, B., & Wisotzki, L. 2004a, *MNRAS*, 352, 399
- Jahnke, K., et al. 2004b, *ApJ*, 614, 568
- Jogee, S. et al. 2008, *ASP Conference Series*, Vol. 396
- Jones, B. & Stein, W. A. 1989, *AJ*, 98, 1557
- Juneau S. et al., 2005, *ApJ*, 619, L135
- Kauffmann, G., et al. 2003a, *MNRAS*, 341, 54
- Kauffmann, G. et al. 2003b, *MNRAS*, 341, 54
- Kauffmann, G. et al. 2003c, *MNRAS*, 346, 1055
- Kauffmann, G., White, S. G., Heckman, T. M., Ménard, B., Brinchmann, J., Charlot, S. Tremonti, C., Brinkmann, J. 2004, *MNRAS*, 353, 713
- Keel, W. C., Kennicutt, R. C., Jr., Hummel, E., & van der Hulst, J. M. 1985, *AJ*, 90, 708
- Keel, W. C. 1993, *AJ*, 106, 1771
- Kennicutt, R. C., Jr., Keel, W. C., van der Hulst, J. M., Hummel, E., & Roettiger, K. A. 1987, *AJ* 95, 5
- Kennicutt, R. C., Jr. 1998, *ARA&A*, 36, 189
- Kennicutt, R. C. & Keel, W. C. 1984, *APJ*, 279, L5
- Kewley, Lisa J., Jansen, Rolf A., Geller, Margaret J. 2005, *PASP*, 117, 227
- Kewley, L., Groves, B., Kauffmann, G., Heckman, T. 2006, *MNRAS*, 372, 961
- Kodama T. et al., 2004, *MNRAS*, 350, 1005
- Kurtz, M. J. & Mink, D. J. 1998, *PASP*, 110, 934
- Lambas, D. G., Tissera, P. B., Alonso, M. S., & Coldwell, G. 2003, *MNRAS*, 346, 1189
- Larson, R. B. & Tinsley, B. M. 1978, *ApJ*, 219, 46
- Le Borgne, D. & Rocca-Volmerage, B. 2002, *A&A*, 386, 446
- Le Fèvre, O. et al. 2005, *A&A*, 439, 845
- Leitherer, C., et al. 1999, *ApJS*, 123, 3
- Letawe, G., Magain, P., Courbin, F., Jablonka, P., Jahnke, K., Meylan, G., & Wisotzki, L. 2007, *MNRAS*, 378, 83
- Li, C., Kauffmann, G., Wang, L., White, S. D. M., Heckman, T. M., & Jing, Y. P. 2006, *MNRAS*, 373, 457
- Li, C. Kauffmann, G., Heckman, T. M., Jing, Y. P., White, S. D. M. 2008a, *MNRAS*, 385, 1903
- Li, C., Kauffmann, G., Heckmann, T. M., White, S. D., & Jing, Y. P. 2008b, *MNRAS*, 385, 1915
- Lin, L. et al. 2007, *ApJL*, 660, L51
- Liske, J., Lemon, D. J., Driver, S. P., Cross, N. J. G., & Couch, W. J. 2003, *MNRAS*, 344, 307
- Liu, C. T. & Kennicutt, R. C., Jr. 1995, *ApJ*, 450, 547
- Makino, J. Hut, P. 1997, *ApJ*, 481, 83
- Markwardt, C. B. 2009, *astro-ph/0902.2850*
- Mignoli, M., et al. 2005, *A&A*, 437, 883
- Mihos, J. C., & Hernquist, L. 1994, *ApJ*, 431, L9
- Mihos, J. C., & Hernquist, L. 1996, *ApJ*, 464, 641
- Mink, D. J.; Wyatt, W. F.; Caldwell, N.; Conroy, M. A.; Furesz, G.; Tokarz, S. P. *Astronomical Data Analysis Software and Systems XVI*, 376, 249
- Nikolic, B., Cullen, H. & Alexander, P. 2004, *MNRAS*, 355, 874
- Noeske K. G. et al., 2007, *ApJ*, 660, L47
- O'Donnell, J. E. 1994, *ApJ*, 422, 1580
- Patton, D. R. et al. 2002, *ApJ*, 565, 208
- Patton, D. R., Grant, J. K., Simard, L., Pritchett, C. J., Carlberg, R. G., & Borne, K. D. 2005, *AJ*, 130, 2043
- Pierce, C. M., et al. 2007, *ApJ*, 660, L19

- Rines .K, Geller M. J., Kurtz M. J. & Diaferio A, 2003, AJ, 126, 2152
- Sánchez, S. F., et al. 2004, ApJ, 614, 586
- Sekiguchi, K. & Wolstencroft, R. D. 1992, 255, 581
- Serber, W., Bahcall, N., Mndard, B., & Richards, G. 2006, ApJ, 643, 68
- Shioya, Y. et al. 2008, ApJS, 175, 128S
- Somerville, R., Hopkins, P. F., Cox, T. J., Robertson, B. E., & Hernquist, L. 2008, MNRAS, accepted
- Smith B. J., Struck C., Appleton P. N., Charmandaris V., Reach W., Eitter J. J., 2005, AJ, 130, 2117
- Spergel, D. et al. 2003, ApJS, 148, 175S
- Springel, V., Di Matteo, T., & Hernquist, L. 2005a, ApJ, 620, L79
- Springel, V., Di Matteo, T., & Hernquist, L. 2005b, MNRAS, 361, 776
- Strateva, I. et al. 2001, AJ, 122, 1861
- Tissera P. B., Domnguez-Tenreiro R., Scannapieco C., & Sàiz A. 2002, MNRAS, 333, 327
- Tran, K.-V. H., et al. 2005, ApJ, 627, L25
- Tremonti C. A. et al., 2004, ApJ, 613, 898
- van Dokkum, P. G. 2005, AJ, 130, 2647
- Vanden Berk, D. E., et al. 2006, AJ, 131, 84
- Vergani, D. et al. 2008, A&A, 487, 89
- Wechsler, R. H., Bullock, J. S., Primack, J. R., Kravtsov, A. V., Dekel, A. 2002, ApJ, 568, 52
- Westra, E., Geller, M. J., Kurtz, M. J., Fabricant, D. G., & Dell'Antonio, I. 2010, ApJ, 708, 534
- Wittman, D. M. et al. 2002, Proc. SPIE, 4836, 73
- Wittman, D., Dell'Antonio, I. P., Hughes, J. P., Margoniner, V. E., Tyson, J. A., Cohen, J. G., Norman, D. 2006, ApJ, 643, 128
- Wolf, C. et al. 2004, A&A, 421, 913
- Wolf, M. J. & Sheinis, A. I. 2008, AJ, 136, 1587
- Woods, D. F., Geller, M. J., & Barton, E. B. 2006, AJ, 132, 197
- Woods, D. F., Geller, M. J. 2007, AJ, 134, 527
- Yee, H. K. C. et al. ApJS, 129, 475
- Yip, C. W., et al. 2004, AJ, 128, 2603
- Zakamska, N. L., et al. 2006, AJ, 132, 1496

This 2-column preprint was prepared with the AAS L^AT_EX macros v5.2.

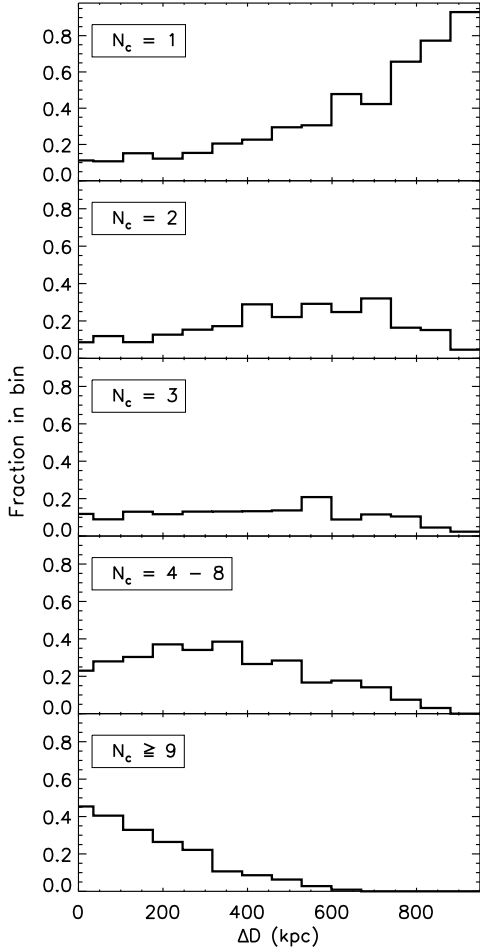


Fig. 12.— Fraction of galaxies in the volume-limited sample with a total N_c neighboring galaxies within 985 kpc co-moving (equivalent to $700 h_{100}^{-1} \text{kpc}$) and $\Delta V < 1000 \text{ km s}^{-1}$ for the volume-limited sample as a function of distance to the nearest neighbor. Pair galaxies have $\Delta D < 70 \text{ kpc}$.

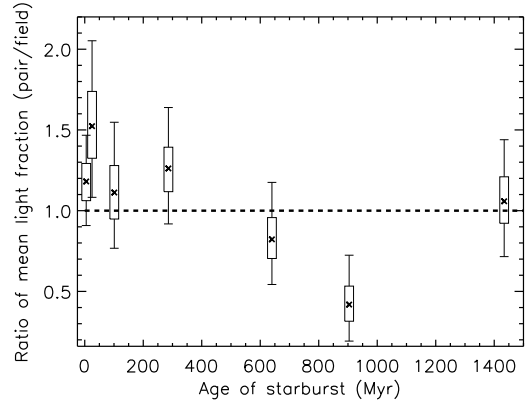


Fig. 15.— Ratio of mean light fraction from starburst populations as a function of starburst population age for pair and unpaired field galaxies with low D_n4000 in the volume-limited sample. The pair galaxies show a greater light fraction from young stellar populations up to burst ages $\sim 300 - 400 \text{ Myr}$. The dashed line indicates a ratio of unity. Error bars are from bootstrap re-sampling: boxes indicate the inter-quartile range and the outer lines show the 95% confidence interval.

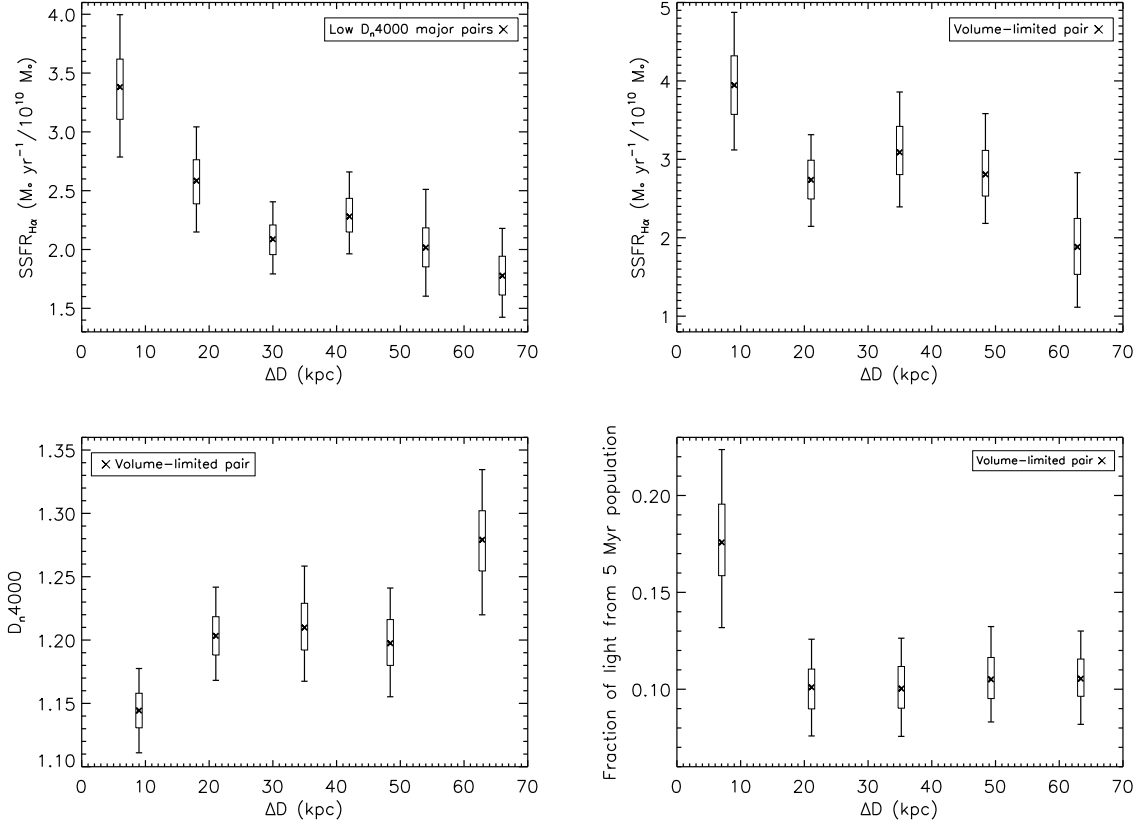


Fig. 13.— Mean star formation indicators versus projected separation. We show the $SSFR_{H\alpha}$ versus projected separation for low D_n4000 major pair galaxies in the full sample at all local densities (*top left*). Star formation indicators for the low D_n4000 galaxies in regions of low local density in the volume-limited major pair sample: $SSFR_{H\alpha}$ (*top right*), D_n4000 (*bottom left*), and fraction of light at 5500 \AA from a 5 Myr starburst population (*bottom right*). Error bars are from bootstrap re-sampling; boxes indicate the inter-quartile range and the outer lines show 95% confidence intervals. For each star formation indicator shown above, the galaxies exhibit a correlation between the star formation indicator and ΔD .

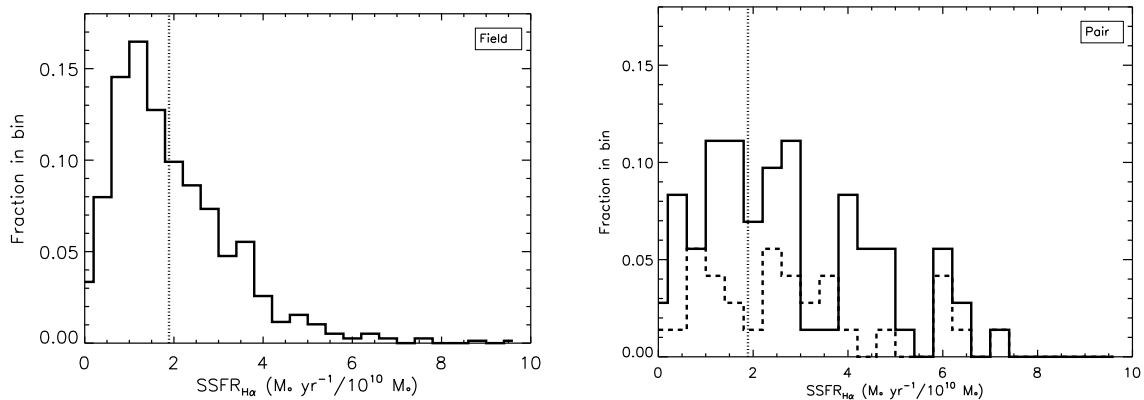


Fig. 14.— Normalized distribution of $\text{SSFR}_{H\alpha}$ for the low D_n4000 pair ($N = 72$) and field galaxies ($N = 777$) in the volume-limited sample. The pair galaxies' distributions exhibit a clear excess of high $\text{SSFR}_{H\alpha}$ compared to that of the field galaxies. The dotted line on both plots indicates the median $\text{SSFR}_{H\alpha}$ for the field galaxies. The dashed line on the pair galaxies' plot shows the contribution from galaxies with $\Delta D < 25$ kpc.